

ENHANCED OPTICAL PERFORMANCE OF TELLURITE GLASS DOPED WITH SAMARIUM NANOPARTICLES FOR FIBER OPTICS APPLICATION

M. N. AZLAN^{a,b,*}, M. K. HALIMAH^c, S. S. HAJER^c, A. B. SURIANI^{a,b},
Y. AZLINA^{a,b}, S. A. UMAR^d

^a*Physics Department, Faculty of Science and Mathematics, Universiti Pendidikan Sultan Idris, 35900 Tanjung Malim, Perak, Malaysia*

^b*Nanotechnology Research Center, Faculty of Science and Mathematics, Universiti Pendidikan Sultan Idris, 35900 Tanjung Malim, Perak, Malaysia*

^c*Physics Department, Faculty of Science, Universiti Putra Malaysia, 43400 UPM Serdang, Selangor, Malaysia*

^d*Department of Physics, Faculty of Science, Bauchi State University Gadau, Nigeria*

We report on the optical efficiency of samarium nanoparticles (NPs) doped tellurite glasses experimentally, for the first time to the best of our knowledge. A high optical efficiency of samarium NPs doped tellurite glasses stable against crystallization was fabricated via melt- quenched technique. In particular, this work underlines the enhancement of optical properties with increasing samarium NPs concentration and the change of polarizability of tellurite glass network with the presence of samarium NPs. Using X-ray diffraction (XRD) analysis, Fourier transform infrared (FTIR) analysis and transmission electron spectra (TEM), the amorphous arrangement, structural assignments and particle size had been revealed. The optical performance of samarium NPs doped tellurite glass was characterized by EL X-02C high accuracy ellipsometer and UV-Vis spectrophotometer. Based on ellipsometer and UV-Vis spectrophotometer, the refractive index was found slightly increases meanwhile the optical band gap is reduced with the presence of samarium NPs. The obtained value of electronic polarizability revealed that samarium NPs affect greatly on polarizability of tellurite glass network. The slightly increases and nonlinear variations of polarizability were found with increasing amount of samarium NPs. The metallization criterion was found to decreased which suggest that the samarium NPs doped tellurite glass tends to be more semiconductor. This is a first step towards high optical performance of tellurite glass with future applications in fiber optics and laser glass.

(Received March 6, 2019; Accepted May 15, 2019)

Keywords: Tellurite glass, Optical band gap, Samarium nanoparticles, Electronic polarizability

1. Introduction

The tellurite glass is important for laser technology due to its numerous excellent properties, such as high transparency, high dielectric constant, high refractive index, low melting point and outstanding nonlinear optical properties [1, 2]. Furthermore, tellurite glass is known to have high solubility with rare earth oxide and low phonon energy. These properties are crucial to develop high optical efficiency of optical fiber. Optical fiber is important in current years especially in remote sensing, laser surgery, long-range laser communications and broadband amplifier [3].

The recent previous research on tellurite laser glass is still rather scarce as it is only deal with rare-earth microparticles [4]. The research on tellurite glass doped with rare earth oxide are

*Corresponding author: azlanmn@fsmt.upsi.edu.my

the most abundant, except research papers dealing with rare earth nanoparticles. Nanomaterials are known to have exceptional optical and electronic properties and these interesting properties are being used in various electronic and optical devices. [5,6]. The unique structure of nanomaterials has opened up a new dimension for development of nanotechnology applications. The nano size particles have been known to give significant effect on semiconductor due to their dependency on size particles [7].

Samarium oxide (Sm_2O_3) is important in optical and electrical applications especially in lasers, phosphors, magnets and thermoelectric device production [4]. Besides that, there is some important and recent research activity concentrated on the study of the optical properties of samarium doped tellurite glass, considered as promising materials for optical fiber, especially in optical amplifier. However, to the best of our knowledge, optical performance of samarium NPs doped tellurite glass has not yet been reported. Comparing with micron size of samarium oxide, the nano size of samarium oxide are of particular interest due to their nano- size effects, interfacial effects, quantum size effects and tunneling effects [8].

Rare earth doped materials have encourage motivation to develop the excellent photonic system for various applications. Samarium oxide is one of the best possible candidates among the lanthanide group in the pursuit for photonic materials research. Samarium comprises of trivalent electron which is known to be advantaged for fiber amplifier applications. Thus, up to date, there is no recent research dealing with samarium NPs doped tellurite glass system, and the current work aims at evaluating this. In this paper, the refractive index and optical absorption of the glass system is revealed to further analyzed the optical band gap energy, electronic polarizability and metallization criterion. The nanoparticles image and the structural parameters are provided.

2. Experimental

A glass series of samarium NPs doped tellurite glasses with good physical and chemical properties are selected as the matrix materials for potential optical fiber. The formulations for the glass series are $\{[(\text{TeO}_2)_{0.7}(\text{B}_2\text{O}_3)_{0.3}]\}_{0.7} [\text{ZnO}]_{0.3}\}_{1-x} \{\text{Sm}_2\text{O}_3\}_x$ (where $y=0.005, 0.01, 0.02, 0.03, 0.04, 0.05$). The glasses were fabricated by via melt-quenching technique. The high purity analytical grade chemicals of samarium (III) oxide nanoparticles, Sm_2O_3 (Alfa Aesar, size particles= 15 nm), tellurium (IV) oxide, TeO_2 (Alfa Aesar), zinc oxide, ZnO (Alfa Aesar), and boron oxide, B_2O_3 (Alfa Aesar) were used to prepare the glass samples. The raw materials were weighed by using digital weighing machine and transferred to alumina crucible. The mixtures in alumina crucible were then transferred to electrical furnace at 900 °C in 2 hours for melting process. The melts were quenched by pouring the molten into stainless steel split molds. The molds were then transferred to the first furnace at 400 °C for 2 hours. The prepared glasses were allowed to be cooled down at room temperature. The prepared glass samples were cut at a thickness of 2 mm by using Isomet Buehler low speed saw machine. The sample was polished with various types of sand papers, 4000 grid, 1500 grid and 1000 grid to acquire smooth surface.

Density of the glass samples were determined by using liquid displacement method of Archimedes principle [18]. Distilled water was used as the immersion liquid and the digital weighing machine was used to calculate the mass of the prepared glass samples. The refractive index of the prepared glass samples was measured by using EL X-02C high precision Ellipsometer with the wavelength of the light source is 632.80 nm and 70° for the angle of occurrence. The optical absorption was recorded by using UV-1650PC UV-Vis Spectrophotometer (Shimadzu) in the wavelength range 190-990 nm. Both refractive index and optical absorption measurement were carried out at room temperature with dark surrounding for better result. All data were analyzed automatically and controlled by a CPU. The data of measurement were calculated by using differential equation for their optical energy gap and absorption coefficient.

3. Results and discussion

X-Ray Diffraction (XRD) and Transmission Electron (TEM)

The x-ray diffraction (XRD) pattern of glass samples were recorded in the range of $\Theta=4^{\circ}$ to $\Theta=86^{\circ}$. The XRD patterns for the various compositions of $\{[(\text{TeO}_2)_{0.7}(\text{B}_2\text{O}_3)_{0.3}]]_{0.7} [\text{ZnO}]_{0.3}\}_{1-x} \{\text{Sm}_2\text{O}_3\}_x$ glasses are shown in Fig. 1. It can be seen from figure that there are no peaks shown which is related to the presence of amorphous structural arrangement in the glass samples. The absence of peaks indicates the non-existence of crystalline phase. The nanoparticle size was confirmed by using transmission electron microscope (TEM) technique. Transmission electron microscope image of samarium NPs doped tellurite glass is shown in Fig. 2. It can be seen clearly from the figure that there is an existence of nanoparticles distribution in the glass sample. From the image, samarium NPs are in the range between 21– 24 nm with the average size of 22.5 nm. The significant increase in size particles after the glass formation is mostly due to the Oswald ripening effect in which the small particle diffuses to larger particle in the glass network [9].

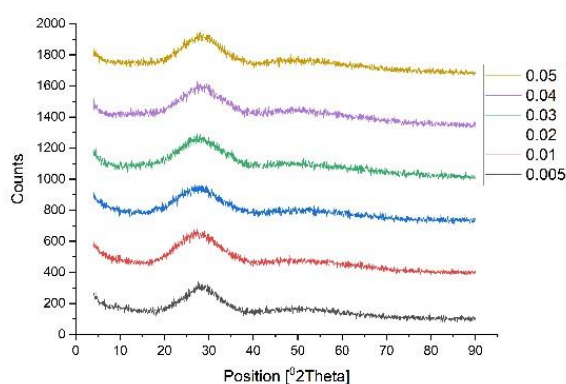


Fig. 1. XRD patterns of samarium NPs doped tellurite glass.

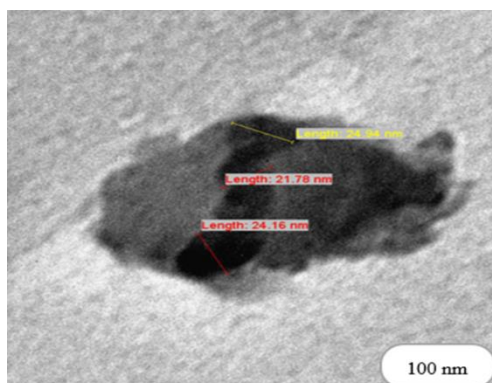


Fig. 2. TEM image of samarium NPs doped tellurite glass.

Fourier Transform Infrared Analysis (FTIR)

FTIR spectroscopy is an important tool for structural characterization and compound identification [10], and it is one of the most common spectroscopic techniques used by organic and inorganic chemists. The main goal of FTIR spectroscopic analysis is to determine the chemical functional groups of the samples [11]. The FTIR spectra for various glass samples samarium NPs doped tellurite glass are shown in Fig. 3. FTIR spectra of all glass samples consist of various absorption bands in different regions lies in between $280 - 2320 \text{ cm}^{-1}$. These bands are influenced by the variation content of samarium NPs because the positions of some absorption bands are

shifted due to compositional variations. The transmission bands of different wavenumbers for all the glass samples are listed in Table 1.

The FT-IR spectra of the present glasses are characterized by intense absorption bands in the frequency regions. The 296-312 cm^{-1} band is assigned to the bending vibrations of zinc oxide, Zn-O linkages [ZnO]. The next bands of 636–649 cm^{-1} corresponds to the TeO_3 trigonal pyramid units [12]. The peaks located in the 1221-1227 cm^{-1} range is assigned to B–O stretching vibrations in BO_3 units from boroxol rings. The absorption band centered at 640 cm^{-1} is the characteristic of pure TeO_2 glass [13–14].

The structural pattern of tellurium containing glasses is determined by trigonal pyramid TeO_3 and bipyramid TeO_4 [15]. The absorption band in the range of 600–700 cm^{-1} in such glasses is due to the stretching vibrations of Te–O bonds in TeO_3 and TeO_4 groups. The absorption of TeO_3 group has a high frequency position than TeO_4 group. The absorption band of TeO_3 group correlates with frequency of 650–700 cm^{-1} and that of TeO_4 group correlated with 600–650 cm^{-1} . The band shifts of these groups depend on changes in the composition of the glass network. Analyzing the obtained results of the present glass system shows that TeO_3 groups are present in all the tellurite containing glasses because of the appearance of the band at 680–728 cm^{-1} [16].

Increasing the B_2O_3 content of the studied glasses generates; (i) a significant increase of the band at 914 cm^{-1} and the shift of this band to 920 cm^{-1} (attributed to the vibrations of the $[\text{BO}_4]$ structural units), (ii) the shift of the band from ~648 to ~617 cm^{-1} (assigned to Te–O bending vibration in $[\text{TeO}_4]$ units), (iii) the shift of the band from ~1243 to ~1254 cm^{-1} and the decrease of intensity (assigned to B–O stretching vibrations in $[\text{BO}_3]$ units from boroxyl rings) and (iv) the shift of the band from ~1428 to ~1437 cm^{-1} and the increase of intensity (attributed to the vibrations of the $[\text{BO}_3]$ units from varied types of borate groups)[17].

Taking into account these changes of the IR spectral features, we assume that the increases of boron trioxide in the glass structure leads to the following: (i) the disintegration of some boroxyl units and the transformation of some trigonal $[\text{BO}_3]$ units into tetrahedral $[\text{BO}_4]$ units and (ii) the number of the $[\text{TeO}_4]$ groups with non-bridging oxygen decrease because some trigonal bipyramidal $[\text{TeO}_4]$ structural units were transformed in trigonal pyramidal $[\text{TeO}_3]$ units [17].

Three broad bands were observed at 296 cm^{-1} , 312 cm^{-1} and 309 cm^{-1} which correspond to ZnO bonding structures. Previous study shows that Zn enter into TeO_2 by the evidence of the vibration and the absorption peaks position shift from 296-309 cm^{-1} [18]. It is also noted that a lot of additional small intensity peaks in the spectra of the glass samples in the range 535-280 cm^{-1} appeared. Those small peaks occur due to the deformation of the Te-O bond vibration [19]. The absorption spectrum of samarium NPs is absent from the transmission spectra which is due to the low concentration of samarium NPs that could not be detected by the instrument.

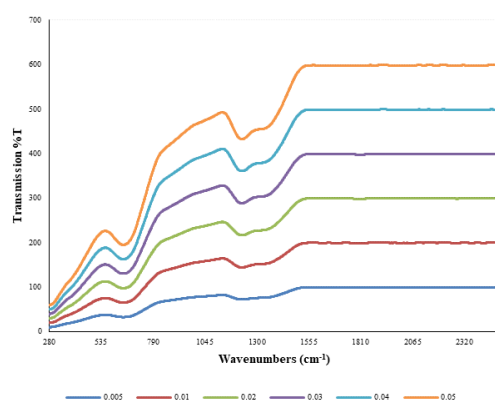


Fig. 3. FTIR spectra of samarium NPs doped tellurite glass.

Table 1. Assignment of infrared transmission bands of samarium NPs doped tellurite glass.

No.	0.005	0.01	0.02	0.03	0.04	0.05	*ASSIGNMENT
1	1226	1226	1224	122 6	122 7	1221	Trigonal B–O stretching vibrations in BO ₃ units from boroxol rings [22]
2	643	649	642	641	644	636	Te–O bending vibrations in [TeO ₃] are exists in all tellurite containing glass [22]
3	-	296	312	309	-	-	ZnO Stretching vibration

Density and Molar volume

The density of glass is a fundamental mechanism required for examining the physical and mechanical state of the glass system. Density was used as a part of figuring of different significant properties, for example, refractive index, elastic properties and thermal conductivity. The density is affected by the structural softening/smallness, changes in geometrical arrangement, coordination number, cross-join thickness and measurement of interstitial spaces of the glass [20].

The density of samarium NPs doped tellurite glass was found in between 3.644 - 4.080 kg m⁻³. The plot of density versus concentration of samarium NPs and their value are shown in Figure 3 and listed in Table 2. The density is shown to be increased with increasing concentration of samarium NPs. This may be due to the increasing number of non-bridging oxygen in the glass system. Another possibility is that the number of atomic mass of samarium which is greater than atomic mass of tellurite contributes to the increasing trend of density. In general, solubility of materials increases in accordance with the decrease of the atomic radius of the rare earth metal [21]. Greenwood reported that, high solubility of the smaller particles results the particles to be distributed uniformly throughout the bulk materials. However, samarium (NPs) has a lower solubility, which results the particles to form a cluster within the glass materials [22]. This will leads to the decreasing number of the density. Azlan et al., found that the high solubility of erbium (NPs) doped tellurite glass results to the higher number of density [23]. However, samarium possesses low solubility, which results to the lower number of density [24].

The plot of molar volume versus concentration of samarium NPs and their value are shown in Fig. 4 and recorded in Table 2. The behavior of molar volume from 0.01 to 0.04 mol fraction is mainly depends upon the density of glasses. The increasing trend of the molar volume is due to the increasing number of oxygen packing density. This will contribute to the increasing compactness of the structure [25]. The increasing behavior of molar volume, V_m is attributed to the changes in molar mass, M with a greater rate than that of density, ρ [26].

The decrease in the molar volume is due to the decreases in the bond length or inter-atomic spacing between the atoms which may be attributed to the increase in the stretching force constants (216 - 217.5 N m⁻¹) of the bonds inside the glass network [19]. Another possibility is that the dual nature of zinc oxide causes the molar volume to decrease with increasing concentration of samarium NPs.

Table 2. Density and molar volume of samarium NPs doped tellurite glass.

Samples	Density (kg/m ³)	Molar Volume (m ³ /mol)
0.005	3.644	32.515
0.010	3.709	32.227
0.020	3.714	32.810
0.030	3.741	33.187
0.040	3.795	33.331
0.050	4.080	31.570

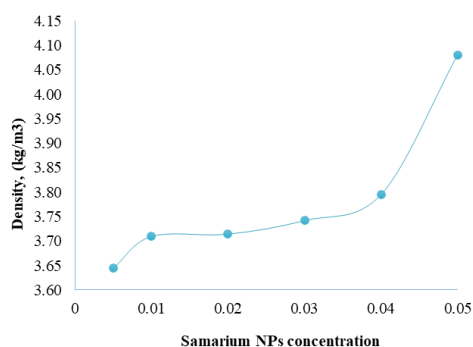


Fig. 4. Density of samarium NPs doped tellurite glass.

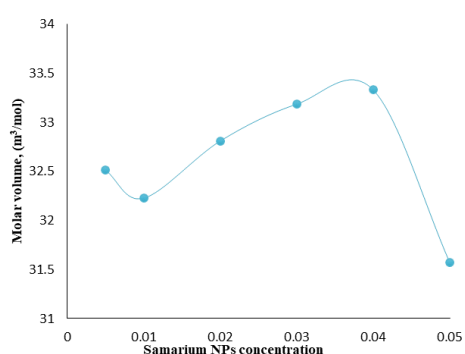


Fig. 5. Molar volume of samarium NPs doped tellurite glass.

Refractive index

Refractive index is used to determine the suitability of materials to be optical devices. Glasses possess excellent optical property which is due to the special structural and intensity distribution. It is well known that the existence of nanoparticles in the materials extend their properties especially in structural and optical performance. Components which influence refractive index are; (i) Polarizability of the first neighbor particles coordinated with its (anion) (ii) Coordination number of the ion (iii) Electronic polarizability of the oxide ion (iv) Optical basicity of the glasses [27].

The values of refractive index for samarium NPs was tabulated in Table 3 and plotted in Fig. 6. It can be seen from Fig. 5 that the refractive index tends to decrease with increasing concentration of samarium NPs up to 0.02 mol fraction of samarium NPs. Meanwhile, the refractive index is suddenly increased at 0.03 - 0.05 mol fraction of samarium NPs. The non-linearity variation of refractive index is due to the variation of structural arrangement in the glass system. The decreasing trend of refractive index is due to the presence of nano size particles that restrict the movement of electrons in the glass system. Besides that, the increasing trend of refractive index is due to the increasing number of density in the glass system.

The refractive index of the glasses does not only depend on the density but also depends on the polarizability of the glass materials [28]. The addition of samarium NPs in the glass system increases the number of non-bridging oxygen. The increasing number of non-bridging oxygen consequently increases the polarizability of the glass system that followed by increasing molar refraction and refractive index [29].

Table 3. Refractive index of samarium NPs doped tellurite glass

Samples	Refractive index(n)
0.005	2.056
0.010	2.011
0.020	2.007
0.030	2.045
0.040	2.050
0.050	2.051

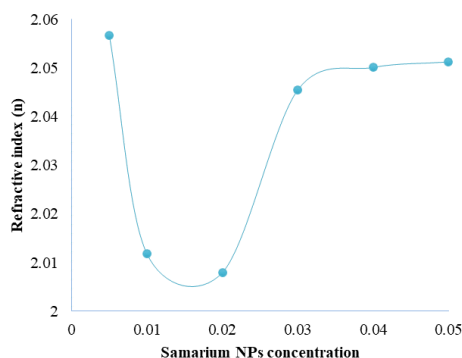


Fig. 6. Refractive index of samarium NPs doped tellurite glass.

Optical absorption

The optical absorption is an important method for investigating optically induced transition to obtain the structural properties of materials [30]. The absorption coefficient $\alpha(\omega)$ is determined at near the absorption edge of all different glass samples and was calculated at different photon energies by using the following relation

$$\alpha = 0.303A/d \quad (1)$$

where A is the absorbance and d is the thickness of the samples. A photon with a certain range of energy can be absorbed by modifying ions in an oxide glasses via either two processes: (i) internal transition between the d-shell electrons or (ii) transfer of an electron from a neighboring atom to the modifier ion and vice versa [31].

The absorption spectra at room temperature for all investigated glasses are shown in Fig. 7. It is obvious that absorption edges of the prepared glasses shift to longer wavelength which is due to the presence of the samarium NPs. The shift increases with increasing concentration of samarium NPs. One possible reason is that there is a change in the glass bonding structure because during melt quenching process from the liquid to the glassy state, the Sm^{2+} ions changed to stable Sm^{3+} ions by taking one electron from oxygen [32] and build new samarium oxide[33]. The absorption edge is affected by the oxygen bond strength in the glass system. The obtained data shows the change of the oxygen bond strength in the glass system. It is observed that the fundamental edge shifts to the longer wavelength with the increase of samarium NPs. This may be due to the less rigidity of the glass system [34].

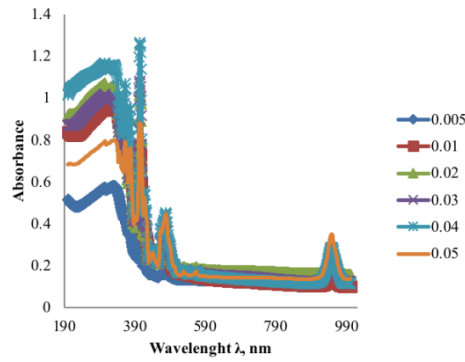


Fig. 7. Optical absorbance spectra of samarium NPs doped tellurite glass.

Optical band gap energy

Energy band gap is a significant method for investigating optically induced transitions and to obtain the properties of the structures and the energy gap (E_g) [30]. Optical transitions are basically two types, direct and indirect transitions. In these transitions, the electromagnetic radiations interact with the electrons in the valence band and reaches to conduction band by gaining fundamental band gap. These transitions occur in both crystalline and amorphous semiconductor materials. These transitions are related with Mott and Davis relation. For photon energies just above fundamental edge, the relation between absorption coefficient (α) and photon energy is given below [35, 36]:

$$\alpha(\omega) = \frac{B(\hbar\omega - E_{opt})^n}{\hbar\omega} \quad (2)$$

where B is a constant related to the extent of the band tailing, $n = 1/2$ for allowed direct transition, $n = 2$ for allowed indirect transition, $\hbar\omega$ is the photon energy and E_g is the optical band gap energy of the material. The optical band gap, E_g , was calculated by extrapolating the linear parts of the curves to $(\alpha\hbar\nu)^{1/2} = 0$ of curve $(\alpha\hbar\nu)^{1/2}$ versus $\hbar\nu$ and extrapolating for the glass samples.

Therefore the Equation (2) for amorphous material becomes

$$(\alpha\hbar\omega)^{1/2} = B(\hbar\omega - E_{opt}) \quad (3)$$

The values of optical band gap E_{opt}^1 and direct optical band gap E_{opt}^2 for samarium NPs doped glass samples can be obtained by extrapolating the straight line on the curve in Fig. 8 to the $(\alpha\hbar\omega)^{1/2} = 0$.

Table 4. Optical band gap energy (E_{opt}^1), and Urbach energy (ΔE) of samarium NPs doped tellurite glass.

Samples	Optical band gap energy, E_{opt}^1 (eV)	Urbach energy, ΔE (eV)
0.005	2.956	0.361
0.010	2.985	0.364
0.020	3.002	0.347
0.030	2.991	0.348
0.040	2.999	0.351
0.050	2.980	0.354

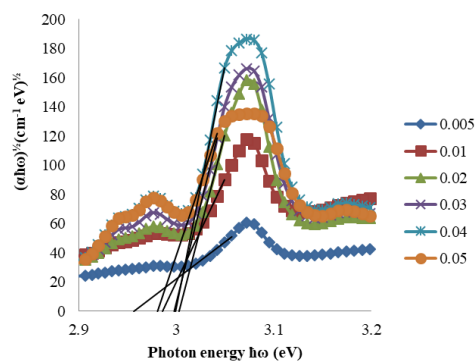


Fig. 8. Plot of $(\alpha\hbar\omega)^{1/2}$ against photon energy $\hbar\omega$ of samarium NPs doped tellurite glass.

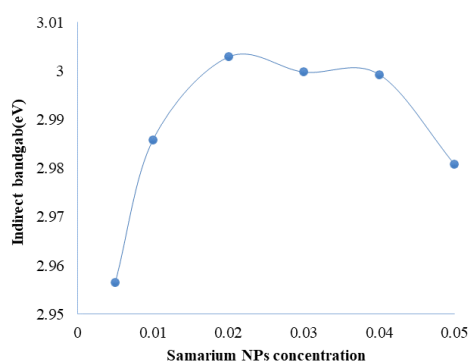


Fig. 9. Optical band gap energy of samarium NPs doped tellurite glass.

Previous research reported that the particles size affects the band gap of the materials [37]. Small size of particles causes the width of both valence and conduction band to decrease. Therefore, the band gap will tend to become wider and results in the increasing value of band gap. (Gupta and Ramrakhiani et al., 2009) reported that the optical properties of materials is highly depends on the size of particles [37]. The band gap increases as the size of particles decreases. It is obvious from the present glass samples that the value of band gap is much higher than that of the reported glass [38]. This is due to fact that the particles size is dependent on the optical properties of materials.

The calculated data of direct and indirect band gap were tabulated and shown in Table 4 and Figs. 9. The indirect band gap is found to be in the range of 2.956–2.980 eV. It can be seen from the Figs. 9 that the band gap of prepared glass samples increases at 0.02 mol fraction and decreases at 0.05 mol fraction along with concentration of samarium NPs.

The change in band gap is due to the shifts of the valence and conduction band from each other [24]. The increasing concentration of samarium NPs leads to the increasing number of non-bridging oxygen. On the other hand, the introduction of samarium NPs in the structure caused the concentration of the tetragonal BO_4 to increase more than the trigonal BO_3 . In general, if there is any change in the oxygen bonding in the glass network, this indicates a change in the information of the absorption features [30]. That gives the possibility of the increasing number of the band gap with increasing concentration of samarium NPs. Moreover, previous research reported that the nanoparticles interrupted the quantum confinement and that increase band gap and photoluminescence. This can be concluded that the band gap energy and photoluminescence depends on the size of particles [39].

The band gap of samarium NPs doped glass was found to be decreased at 0.05 mol fraction with an increase of samarium NPs [30]. This behavior can be explained by the structural changes in the glass system [24]. Another possibility is that the attribution to the variation of

density and the non-bridging oxygens in the glass structure. The broadening of the valence band or multivalence structures in the presence of Sm electrons leads to metallization of the glasses. The glasses will be more conductive compared to the undoped glass because electrons in the valence band can easily move to the conduction band. Interestingly, the optical energy band gap E_{opt} of the glasses is strongly sensitive to the concentration of the natural samarium NPs [29].

It is well known that samarium and boron have more than one stable electronic configuration. As the content of samarium NPs increases, the bond length of BO_3 structural units is increased. This is in accordance to the direct proportionality to the molar volume and the formation of NBO. These factors are responsible of the decreasing value of band gap energy in the glass system [24].

Urbach energy

An exponentially increasing absorption coefficient with photon energy near the absorption edge of amorphous materials is very interesting phenomena to be studied. When an incident photon on the materials has energy less than band gap energy of the materials, the increasing absorption coefficient is followed with an exponential decay of state density localized into the gap [40]. The lack of crystalline long-range order in amorphous or glassy materials is associated with a tailing of states density into normally forbidden energy [41, 42]. The exponentially increasing absorption edge in a number of insulators including crystalline and non-crystalline semiconductors follows the empirical expression described by the Urbach rule [42, 43]

$$\alpha(\nu) = \beta \exp\left(\frac{h\nu}{\Delta E}\right) \quad (4)$$

where β is a constant, h is the Plank constant, ν is the photon frequency and ΔE is the Urbach energy or Band tail. The Urbach energy ΔE can be easily determined from linear relation between $\ln(\alpha)$ and $h\nu$. ΔE values are calculated by taking inverse of the Urbach's tail slopes $\ln \alpha$ in the lower photon energy region of the curve [33]. The relation between $\ln(\alpha)$ and $h\nu$ of the glass samples is shown in Fig. 10.

The Urbach energy data of the prepared glass samples is tabulated and shown in Table 4 and Fig. 11. The Urbach energy values of the prepared glasses are found in the range 0.361–0.354 eV. It is known that materials which possess large value of Urbach energy have higher tendency to convert the weak bonds into defects. It can be seen that the Urbach energy increases as the content of samarium NPs oxide increases. This is probably due to the increase in the TeO_4 pyramids as the content of samarium NPs oxide increases. The presence of TeO_4 pyramids results in less stable structure and lower connectivity in the glass network [35]. It can be seen that the Urbach energy tends to decrease with increasing concentration of the samarium NPs at 0.02 mol fraction. Consequently, the width of the state density localized in the forbidden gap become smaller and the density of electrons with higher energy is reduced due to the electronic transition from the valence band to the conduction band [40]. More probably, the glasses with the smaller Urbach energy would have greater tendency to minimize the static disorder in the glass structure [29].

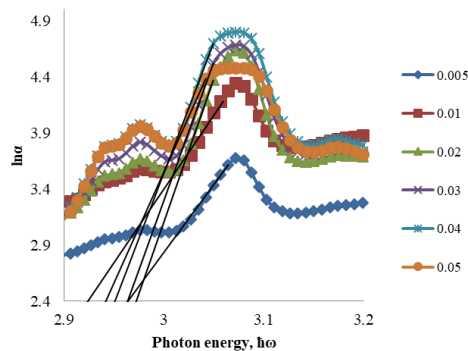


Fig. 10. Variation of $\ln(\alpha)$ with photon energy $h\nu$ (eV) of samarium NPs doped tellurite glass

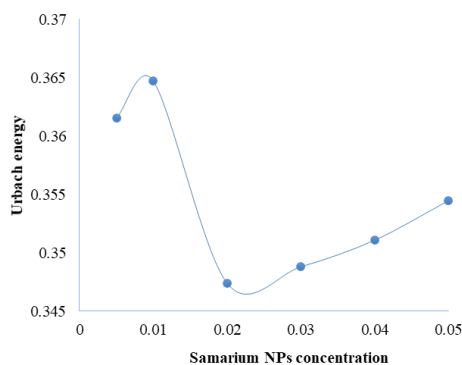


Fig. 11. Urbach energy of samarium NPs doped tellurite glass.

Electronic polarizability

The molar refraction value can be calculated from Lorentz-Lorenz relationship by the following equation [44]:

$$R_m = \frac{(n_0^2 - 1)}{(n_0^2 + 2)} V_m \quad (5)$$

where n_0 is the refractive index and V_m is the molar volume. The value of electronic polarizability can be calculated by substitute the value of Avogadro's number to the Lorentz- Lorenz relationship as follows [44]:

$$\alpha_m = \frac{3}{4\pi N_A} R_m \quad (6)$$

where the symbol of N_A is referring to Avogadro's number which represent the number of polarizable ions per mole. The equation (6) can be rearranged to the following expression [45]:

$$\alpha_m = \frac{R_m}{2.52} \quad (7)$$

where α_m is the value of average polarizability. Based on Lorentz-Lorenz equation, the value of electronic polarizability is calculated and listed in Table 5. The trend of electronic polarizability along with samarium NPs concentration is shown in Fig. 12. It can be seen from the figure that the trend of electronic polarizability is nonlinear along with samarium NPs concentration. The decrease of polarizability at 0.01 and 0.05 indicates the reduction of mobility of electron in the glass system. Such trend might be due to the structural change originated from the decrease in the number of nonbridging oxygen [46]. However, the number of electronic polarizability is found increases from 0.01 – 0.04 of samarium NPs concentration.

The deformability of electron cloud is affected by the number of non-bridging oxygen exists in the glass system. Non-bridging oxygen consists of free electrons from the lone pair which are less tightly bound to the nuclear charge [44]. Consequently, the free electrons are easily polarized as the electrical field is penetrated through the medium. The formation of non- bridging oxygen ions of both dopants is confirmed from the formation of TeO_3 and BO_3 structural units as shown from FTIR results. The number of non-bridging oxygen ions is increased as the concentration of samarium NPs increases. The increment number of non- bridging oxygen leads to the raised number of free electrons in the glass system [45]. Hence, the electronic polarizability is increased as the concentration of samarium NPs increases.

Table 5. Electronic polarizability of samarium NPs doped tellurite glass.

Samples	Electronic Polarizability, a_e (\AA^3)
0.005	6.686
0.01	6.440
0.02	6.540
0.03	6.778
0.04	6.829
0.05	6.472

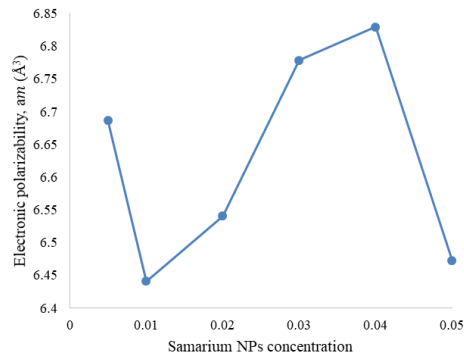


Fig. 12. Electronic polarizability of samarium NPs doped tellurite glass.

Metallization criterion

The nature of metallic and non-metallic of glass system can be predicted by the following conditions: $R_m/V_m < 1$ (non-metal) and $R_m/V_m > 1$ (metal). The value of metallization criterion can be calculated from the basis of Lorentz-Lorenz equation by the following equation [47]:

$$M = 1 - \frac{(n_0^2 - 1)}{(n_0^2 + 2)} \quad (8)$$

where n_0 is the value of refractive index. The calculated values of metallization criterion for the glass samples are tabulated in Table 6 and plotted in Fig. 13. It can be seen from figure that the value of metallization criterion is increased from 0.005 – 0.02 concentration of samarium NPs. Such trend indicates that the samples are not metalizing and the width of conduction bands becomes smaller [47]. Furthermore, the increase of metallization criterion leads to the increase tendency to be more insulator and non-metallic.

The increase in metallization criterion reflects to the value of optical band gap energy which increases from 0.005 – 0.02 concentration of samarium NPs. Meanwhile, the value of metallization criterion starts to drop from 0.03 – 0.05 concentration of samarium NPs. This trend is due to the decrease in forbidden gap and the widen of conduction band in energy level. The reduction of metallization criterion corresponds to the increase tendency towards conductivity and metallic [44]. Moreover, the increase in metallization criterion indicates that the glass system is metalizing and increase tendency to be more semiconductor.

Table 6. Metallization criterion of samarium NPs doped tellurite glass.

Samples	Metallization Criterion
0.005	0.481
0.01	0.496
0.02	0.497
0.03	0.485
0.04	0.483
0.05	0.483

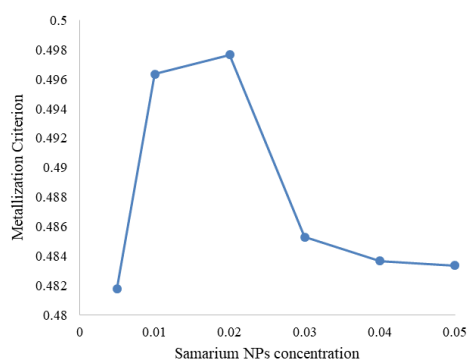


Fig. 13. Metallization criterion of samarium NPs doped tellurite glass.

4. Conclusions

The amorphous nature of the glass samples was confirmed by X-ray diffraction (XRD) method. The presence of Sm_2O_3 (NPs) was confirmed by using TEM technique with an average size of 22.5 nm. The FTIR spectra revealed the structural parameters of tellurite oxide and borate oxide which proved the existence of nonbridging oxygen. The density of the glass samples was enhanced with an increase of samarium NPs which is due to the low solubility of samarium NPs. The molar volume of samarium NPs doped tellurite glass is reduced with increasing amount of samarium NPs due to the dual nature of zinc oxide. The refractive index of these glasses was decreased at 0.02 mol fraction of samarium NPs which is due to the restriction movement of the electrons with respect to their small size of particles. The refractive index was found highest at 5 mol fraction of samarium NPs which is due to the high concentration of non-bridging oxygen. The absorption edge is found shifted to longer wavelength.

The decrease in optical band gap energy is due to the broadening of the valence band or multivalence structures in the presence of samarium NPs electrons. Urbach energy values of the prepared glasses are found in the range 0.347– 0.354 eV. It is known that materials which possess large value of Urbach energy have higher tendency to convert the weak bonds into defects. The electronic polarizability was found maximum at 0.04 mol fraction of samarium NPs which indicates the highest possibility for the glass materials to be applied in nonlinear optical applications. The lowest value of metallization criterion was found at 0.05 mol fraction of samarium NPs which correspond to the high tendency of glass materials to be applied in semiconductors applications. Based on these results, the novel samarium NPs doped tellurite glass has high possibility for high optical performance of fiber optics and excellent lasing materials.

Acknowledgments

The writers appreciate the financial support for the work from the Ministry of Higher Education of Malaysia and Universiti Pendidikan Sultan Idris through Skim Geran Penyelidikan Fundamental, FRGS (Code: 2019-0006-102-02 (FRGS/1/2018/STG07/UPSI/02/1)) and Geran Penyelidikan Universiti, GPU (Code: 2018-0139-103-1). The authors would like to thank the following institutions for equipment support: Faculty of Science and Mathematics, Universiti Pendidikan Sultan Idris and Faculty of Science, Universiti Putra Malaysia.

References

- [1] M. N. Azlan, M. K. Halimah, *Results in Physics* **11**, 58 (2018).
- [2] N. N. Yusof, S. K. Ghoshal, M. N. Azlan, *Journal of Alloys and Compounds* **724**, 1083 (2017).
- [3] C. Eevon, M. K. Halimah, A. Zakaria, C. A. C. Azurahaman, M. N. Azlan, M. F. Faznny, *Results in Physics* **6**, 761 (2016).
- [4] Sevcan Tabanlı, Gonul Eryurek, *Sensors and Actuators A: Physical* **285**, 448 (2019).
- [5] A. P. Alivisatos, *Semiconductor Clusters, Nanocrystals and Quantum Dots,* *Science* **271**(5251), 933 (1996).
- [6] R. J. Ellingson, M. C. Beard, J. C. Johnson, P. Yu, O. I. Micic, A. J. Nozik, A. Shabaev, A. L. Efros, *Nano Lett.* **5**(5), 865-71 (2005).
- [7] A. Linsebigler, G. Lu, J.T. Yates, Jr, *J. Phys. Chem.* **99**, 7626 (1995).
- [8] W. Zhu, L. Xu, J. Mab, R. Yang, Y. Chen, *Journal of Colloid and Interface Science* **340**(1), 119(2009).
- [9] M. S. A. Mohd Saidi, S. K. Ghoshal, K. Hamzah, R. Arifin, M. F. Omar, M. K. Roslan, E. S. Sazali, *Journal of Non-Crystalline Solids* **502**, 198 (2018).
- [10] S. Hsu, "Separation Sciences Research and Product Development," Mallinckrodt Baker Division, Mallinckrodt, Inc".
- [11] C. R. Gautam, A. K. Yadav, *Optics and Photonics Journal* **3**, 1 (2013).
- [12] Rada E. Culeva, V. Rus, M. Pica, M. Culea, *Journal of Materials Science* **43**, 3713 (2008).
- [13] R. A. El- Mallawamy, *Infrared Phys.* **29**(2-4), 781 (1989).
- [14] M. El-Zaidia, A. Ammar, El-Mallawamy, *Physica Status Soli (a)* **91**, 637 (1985).
- [15] P. G. Pavani, K. Sadhana, V. C. Mouli, *Journal of Physica B* **406**(6-7), 1242 (2011).
- [16] R. C. Lucacel, I. Ardelean, *J. Optoelectron. Adv. M.* **8**(3), 1124 (2006).
- [17] S. Rada, M. Culea, E. Culea, *Journal of Non-Crystalline Solids* **354**, 5491 (2008).
- [18] H. A. A Sidek, S. P. Chow, Z. A. Talib, S. A. Halim, *Turk. J. Phys.* **28**, 65 (2004).
- [19] H. A. A. Sidek, S. Rosmawati, Z. A. Talib, M. K. Halimah, W. M. Daud, *American Journal of Applied Sciences* **8**, 1489 (2009).
- [20] S. Rada, A. Dehelean, E. Culea, *Journal of Non-Crystalline Solids* 3070 (2011).
- [21] L. L. Rokhlin, *Journal of Phase Equilibria* **19**(2), 142 (1998).
- [22] G. W. Greenwood, *The growth of dispersed precipitates in solutions. Acta metallurgica* **4**, 1956.
- [23] M. N. Azlan, M. K. Halimah, H. A. A. Sidek, *Journal of Luminescence* **181**, 400 (2017).
- [24] M. N. Azlan, M. K. Halimah, S. Z. Shafinas, W. M. Daud, *Journal of Nanomaterials* **2013**, 1 (2013).
- [25] B. Eraiah, G. Sudha, Bhat, *Journal of Physics and Chemistry of Solids* **68**, 581 (2007).
- [26] Y. B. Saddeek, M. S. Gaafar, *Journal of Materials Chemistry and Physics* **115**, 280 (2009).
- [27] E. Yousef, B. Al-Qaisi, *Journal of Solid State Sciences* **19**, 6 (2013).
- [28] M. Abdel-Baki, F. El-Diasty, F. A. A. Wahab, *Optical Communications* **261**, 65 (2006).
- [29] W. Widanarto, M. R. Sahar, S. K. Ghoshal, R. Arifin, M. S. Rohani, K. Hamzah, M. Jandra, *Materials Chemistry and Physics* **138**, 174 (2013).
- [30] H. Aboud, H. Wagiran, I. Hossain, *Journal of Materials Letters* **85**, 21 (2012).
- [31] Y. Wang, S. Dai, F. Chen, *Journal of Materials, Chemistry and Physics* **113**, 407 (2009).

- [32] J. Tauc, *Materials Research Bulletin* **5**(8), 721 (1970).
- [33] W. Widanarto, M. R. Sahar, S. K. Ghoshal, R. Arifin, M. S. Rohani, K. Hamzah, *Journal of Magnetism and Magnetic Materials* **326**, 123 (2013).
- [34] M. K. Halimah, W. M. Daud, H. A. A. Sidek, A. W. Zaidan, *Materials Science- Poland* **28**(1), 173 (2010).
- [35] E. A. Davis, N. F. Mott, *Philosophical Magazine* **22**(179), 903.
doi:10.1080/14786437008221061, 1970.
- [36] B. Eraiah, *Bulletin of Material Science* **29**(4), 375. doi:10.1007/BF02704138. 2006.
- [37] P. Gupta, M. Ramrakhiani, *The Open Nanoscience Journal* **3**, 15 (2009).
- [38] Z. A. S. Mahraz M. M. R. Sahar, S. K. Goshal, *Journal of Luminescence* **144**, 139 (2013).
- [39] K. M. Reddy, S. V. Manorama, A. R. Reddy, *Materials Chemistry and Physics* **78**, 239 (2002).
- [40] I. Jlassi, H. Elhouichet, M. Ferid, *Journal of Materials Science* **46**(3), 806 (2011).
- [41] A. Kaur, A. Khanna, C. Pesquera, F. Gonzalez, V. Sathe, *Journal of Non-Crystalline Solids* **356**, 864 (2010).
- [42] N. A. Zarifah, M. K. Halimah, M. Hashim, B. Z. Azmi, W. M. Daud, *Chalcogenide Letters* **7**, (9), 565 (2010).
- [43] R. K. Singh, A. Srinivasan, *Journal of Magnetism and Magnetic Materials* **323**, 330 (2011).
- [44] M. K. Halimah, M. F. Faznny, M. N. Azlan, H. A. A. Sidek, *Results in Physics* **7**, 581 (2017).
- [45] Y. J. Cha, J. H. Kim, J.-H. Yoon, B. S. Lee, S. Choi, K. S. Hong, E. D. Jeong, T. Komatsu, H. G. Kim, *Journal of Non-Crystalline Solids* **429**, 143 (2015).
- [46] Yukina Taki, Kenji Shinozaki, Tsuyoshi Honma, Vesselin Dimitrov, Takayuki Komatsu, *Journal of Solid State Chemistry* **220**, 191 (2014).
- [47] M. N. Azlan, M. K. Halimah, S. Z. Shafinas, W. M. Daud, *Materials Express* **5**(3), 2015.